J. Fluid Mech. (1965). *vol.* 23, *part* 3, *pp.* 521–544
Printed in Great Britain

On spatially growing disturbances in an inviscid shear layer

By A. MICHALKE

Deutsche Versuchsanstalt für Luft- und Raumfahrt e.V.,
Institut für Turbulenzforschung, Berlin

(Received 19 April 1965)

Experimental investigations of shear layer instability have shown that some obviously essential features of the instability properties cannot be described by the inviscid linearized stability theory of temporally growing disturbances. Therefore an attempt is made to obtain better agreement with experimental results by means of the inviscid linearized stability theory of spatially growing disturbances. Thus using the hyperbolic-tangent velocity profile the eigenvalues and eigenfunctions were computed numerically for complex wave-numbers and real frequencies. The results so obtained showed the tendency expected from the experiments. The physical properties of the disturbed flow are discussed by means of the computed vorticity distribution and the computed streaklines. It is found that the disturbed shear layer rolls up in a complicated manner. Furthermore, the validity of the linearized theory is estimated. The result is that the error due to the linearization of the disturbance equation should be larger for the vorticity distribution than for the velocity distribution, and larger for higher disturbance frequencies than for lower ones. Finally, it can be concluded from the comparison between the results of experiments and of both the spatial and temporal theory by Freymuth that the theory of spatially-growing disturbances describes the instability properties of a disturbed shear layer more precisely, at least for small frequencies.

1. Introduction

This paper is concerned with the hydrodynamic instability of boundary layers that are not bounded by walls and, therefore, are called free boundary layers or shear layers. They occur in jets and wakes, and a characteristic feature of these velocity profiles is that they have inflexion points.

It has already been shown by Rayleigh (1880) that velocity profiles with inflexion points in an inviscid fluid are unstable relative to certain wavy disturbances. The instability mechanism of free boundary layers is an inviscid one, caused by induction effects, and viscosity has only a damping influence (cf. Lin 1955). Furthermore, for large Reynolds numbers the flow in a free boundary layer is nearly parallel. Thus results obtained by means of the inviscid linearized stability theory for unidirectional flow may then be applied to free boundary layers at large Reynolds numbers.

Stability calculations for special shear layers at finite Reynolds numbers by

Lessen (1950), Esch (1957) and Betchov & Szewczyk (1963) have in fact shown that for large Reynolds numbers the neutral curve approaches asymptotically the neutral value predicted by inviscid theory and that for finite Reynolds numbers the amplification of disturbances is always smaller than in the inviscid case. The same result was obtained by Tatsumi & Kakutani (1958), who dealt with the instability of a plane jet. Also experimental investigations of free boundary layers of plane and axisymmetric jets carried out by Sato (1960), Schade & Michalke (1962) and Michalke & Wille (1965) have shown that for large Reynolds numbers the instability properties of free boundary layers are not noticeably affected by viscosity. Furthermore, it was found by Michalke & Schade (1963) that, as far as the instability at infinite Reynolds number is concerned, jet boundary layers behave like a single shear layer, if the width of the jet core is large compared with the thickness of the jet boundary layer. Experimental results obtained from jet boundary layers that satisfy this condition may then be compared with theoretical results for shear layers provided that the velocity profiles are comparable in both cases.

A shear layer at large Reynolds numbers was investigated by Sato (1956, 1959), using a hot-wire technique. He found that artificial disturbances excited by sound from a loudspeaker grow exponentially with downstream distance in the first stage. In order to compare the evaluated growth rates with theoretical results obtained from the inviscid linearized stability theory of Lessen (1950) for a special shear layer, Sato transformed linearly the time-dependent growth rate of the disturbances assumed in the theory into a spatial growth rate by means of the disturbance phase velocity. This transformation was first used by Schubauer & Skramstad (1947). Sato found that the measured growth rates were of the same order of magnitude as the transformed theoretical ones. Concerning the phase velocity the agreement was equally good. Also Sato (1959) measured the amplitude distribution of the velocity fluctuations. As long as the disturbances grew exponentially, showing that the linearized theory was applicable, the fundamental component of the velocity fluctuation—which should be equivalent to the disturbance velocity component in the basic flow direction—showed a phase reversal; i.e. it became zero at one point. This phase reversal was, however, not placed at the critical layer, but far outside in a region where the velocity of the basic flow was small. Contrary to this the theoretical amplitude distribution of the neutral disturbance—the only one available to Sato—had a phase reversal at the critical layer. Sato supposed that better agreement would be expected using the eigenfunctions of (temporally) amplified disturbances.

A similar distribution of velocity fluctuations was observed by Wehrmann & Wille (1958) in a disturbed axisymmetric jet boundary layer the thickness of which was small compared with the width of the jet core. Wehrmann (1960) and Fabian (1960) explained this distribution of velocity fluctuation which showed also a distinct phase reversal with the existence of ring vortices in the jet boundary layer. An attempt to explain the formation of vortices in a free boundary layer by means of the inviscid linearized stability theory was made by Schade & Michalke (1962). They approximated a measured boundary-layer profile of the axisymmetric jet by a linear broken-line profile so that the maximum slope of

both profiles was the same. The comparison of the wave-numbers for temporally amplified disturbances of the broken-line profile with the measured values showed relatively good agreement. But the experimental results showed that there was no strict proportionality between wave-number and disturbance frequency, contrary to the theory. Therefore the measured phase velocity depended also on the frequency, while in the theory it was constant.

The amplification of artificially excited disturbances in plane and axisymmetric jet boundary layers was investigated by Michalke & Wille (1965). In both cases an exponential growth of the disturbances with increasing downstream distance was found. But, if the above-mentioned space–time transformation was used, the comparison of these growth rates with the theoretical ones of the corresponding broken-line profile showed only order-of-magnitude agreement. It was supposed that the difference in the results was caused by the very rough approximation of the measured velocity profile by a linear broken-line profile. Therefore a stability calculation according to inviscid linearized theory was carried out by Michalke (1964) using the smooth hyperbolic-tangent velocity profile, which is a very good approximation to the measured jet boundary-layer profiles. For temporally amplified disturbances the eigenvalues and eigenfunctions were computed numerically. The result, however, was disappointing: application of the tanh profile yielded no better agreement between theory and experiment, although in the meantime more detailed and improved measurements had been presented by Freymuth (1965). Contrary to the experimental results the calculation yielded proportionality between the wave-number and the frequency and a constant phase velocity. For the fundamental component of the velocity fluctuation the discrepancy was still larger. Only for the neutral disturbance did a phase reversal occur, and this at the critical layer, i.e. at the location of the inflexion point. For temporally amplified disturbances, however, the theory does not yield a phase reversal at all, while for the spatially amplified disturbances in the experiment a phase reversal is found. Thus the question arose as to what caused these discrepancies. One reason was supposed to lie in the variation of the velocity profile in the near neighbourhood of the nozzle by which the jet was generated. There the boundary-layer profile at the nozzle wall changes into the free boundary-layer profile of the jet. This is connected with a strong shift in the position of the inflexion point of the velocity profile. But from his thorough experimental investigation of jet boundary-layer instability Freymuth (1965) came to the conclusion that the reason lies in the fact that the amplification of disturbances in free boundary layers can only be described by a stability theory for spatially growing disturbances. Watson (1962) had made the same suggestion for plane Poiseuille flow. He developed a non-linear stability theory for spatially growing disturbances.

Furthermore, from theoretical considerations, Gaster (1962) came to the conclusion that the growth rates obtained from a stability calculation for temporally growing disturbances cannot be transformed linearly with the phase velocity into spatial growth rates. For weak amplification only, a transformation is possible by means of the group velocity. In a further paper Gaster (1965) showed that for strongly spatially amplified disturbances as present in shear layers the

eigenvalue equation has to be solved for complex wave-numbers in order to evaluate the spatial growth rate, and he carried out the calculation for the linear broken-line velocity profile. Gill (1965) investigated the stability of spatially damped disturbances of Poiseuille flow in a tube and found good agreement with the experimental results of Leite (1956).

In order to compare the instability properties of spatially growing disturbances in an inviscid shear layer with those of temporally growing disturbances an inviscid stability calculation for the hyperbolic-tangent velocity profile was carried out under the assumption of spatially growing disturbances. The results are reported below.

2. The inviscid linearized disturbance equation in the two-dimensional case

For reasons which will become evident later the inviscid linearized disturbance equation will be derived here in more detail. The flow of an inviscid fluid is governed in the two-dimensional case by the Helmholtz vorticity equation

$$\frac{d\Omega}{dt} = \frac{\partial\Omega}{\partial t} + u\frac{\partial\Omega}{\partial x} + v\frac{\partial\Omega}{\partial y} = 0. \tag{1}$$

Here $u(x, y, t)$ and $v(x, y, t)$ denote the x- and y-components of the velocity vector

$$\mathbf{c} = (u, v, 0), \tag{2}$$

and $\Omega(x, y, t)$ denotes the z-component of the vorticity defined by

$$\operatorname{curl}\mathbf{c} = (0, 0, \Omega). \tag{3}$$

Thus (2) yields

$$\Omega = \partial v/\partial x - \partial u/\partial y. \tag{4}$$

Suppose now a unidirectional steady basic flow is given by its velocity profile $U(y)$ and its vorticity distribution

$$\Omega_0(y) = -U', \tag{5}$$

where the prime denotes differentiation with respect to y. Further, let us superimpose a small disturbance $\epsilon u_1(x, y, t)$, $\epsilon v_1(x, y, t)$ and $\epsilon\Omega_1(x, y, t)$ upon this basic flow. Then inserting

$$\left.\begin{aligned} u(x, y, t) &= U(y) + \epsilon u_1(x, y, t), \\ v(x, y, t) &= \epsilon v_1(x, y, t), \end{aligned}\right\} \tag{6}$$

$$\Omega(x, y, t) = \Omega_0(y) + \epsilon\Omega_1(x, y, t) \tag{7}$$

into (1) we obtain, using (5),

$$\epsilon\,\partial\Omega_1/\partial t + [U + \epsilon u_1]\,\epsilon\,\partial\Omega_1/\partial x - \epsilon v_1[U'' - \epsilon\,\partial\Omega_1/\partial y] = 0. \tag{8}$$

ϵ is a measure of the magnitude of the disturbance. In general the solution of this non-linear disturbance equation (8) will depend on the disturbance magnitude ϵ. Only if

$$U \gg |\epsilon u_1|; \quad |U''| \gg |\epsilon\,\partial\Omega_1/\partial y|, \tag{9}$$

can the disturbance terms in the brackets of (8) be neglected, and can we obtain the linearized disturbance equation

$$\partial\Omega_1/\partial t + U\,\partial\Omega_1/\partial x - U''v_1 = 0, \tag{10}$$

the solution of which depends on ϵ no more. In the following analysis the conditions (9) are assumed valid. Introducing a stream function $\psi_1(x, y, t)$ by

$$u_1 = \partial\psi_1/\partial y, \quad v_1 = -\partial\psi_1/\partial x, \tag{11}$$

we can satisfy the continuity equation. If we restrict ourselves to wavy disturbances

$$\left.\begin{aligned}\psi_1(x, y, t) &= \mathscr{R}\{\phi(y)\, e^{i(\alpha x-\beta t)}\},\\ \Omega_1(x, y, t) &= \mathscr{R}\{\omega(y)\, e^{i(\alpha x-\beta t)}\},\end{aligned}\right\} \tag{12}$$

where α and β are constants, equations (11), (10) and (4) yield

$$\left.\begin{aligned}(\alpha U-\beta)\,\omega+\alpha U''\phi &= 0,\\ \omega &= -[\phi''-\alpha^2\phi],\end{aligned}\right\} \tag{13}$$

or, by elimination of ω, the Rayleigh equation

$$(U-\beta/\alpha)\,[\phi''-\alpha^2\phi]-U''\phi = 0, \tag{14}$$

is obtained. For unbounded velocity profiles the disturbances must vanish at infinity, so the boundary conditions are

$$\phi(-\infty) = \phi(+\infty) = 0. \tag{15}$$

Since the velocity profile is unbounded,

$$\lim_{y\to\pm\infty} U'' = 0, \tag{16}$$

and from (14) and (15) the asymptotic behaviour of ϕ for $y \to +\infty$ is

$$\phi' = -\alpha\phi \tag{17}$$

and for $y \to -\infty$ is

$$\phi' = \alpha\phi. \tag{18}$$

The order of the differential equation (14) can be reduced if we set

$$\phi = \exp\left[\int \Phi\, dy\right]. \tag{19}$$

Thus we obtain from (14) the corresponding Riccati equation in $\Phi(y)$

$$\Phi' = \alpha^2 - \Phi^2 + U''/(U-\beta/\alpha). \tag{20}$$

With (17) and (18) the appropriate boundary conditions become

$$\Phi(+\infty) = -\alpha; \quad \Phi(-\infty) = +\alpha. \tag{21}$$

The constants $\alpha = \alpha_r + i\alpha_i$ and $\beta = \beta_r + i\beta_i$ are in general complex. α_r is the wave-number, β the cyclic frequency or angular velocity of the disturbance and α_i and β_i the spatial and temporal growth rates respectively. Without loss of generality we can assume $\beta_r > 0$. If we put $\alpha_i = 0$, then the amplitude of the disturbance depends only on y and t. This may be called the timewise case after Gill (1965). On the other hand, for $\beta_i = 0$ we have the spacewise case. For the neutral disturbance $\alpha_i = \beta_i = 0$ and both cases have the same solution.

The basic flow whose instability is investigated here is given by the velocity profile

$$U(y) = 0{\cdot}5[1+\tanh y]. \tag{22}$$

All quantities used here and in the following (except in the appendix) are assumed to be normalized with the maximum velocity U_0 of the shear layer and a length scale L. The instability properties for the timewise case of this velocity profile (22) were calculated by Michalke (1964). In the following we shall treat the spacewise case.

3. Evaluation of the eigenvalues for the spacewise case

In order to study the instability properties of the tanh velocity profile (22) in the spacewise case we have to integrate the differential equation (14) or (20) with the boundary conditions (15) and (21) respectively for real values $\beta > 0$. We therefore have to solve an eigenvalue problem in order to determine

$$\alpha = \alpha(\beta) = \alpha_r + i\alpha_i.$$

For the neutral case $\alpha_i = 0$ the eigenvalues are well known. They are $\alpha_r = 1$ and $\beta = 0{\cdot}5$, and the eigenfunction $\phi = \operatorname{sech} y$. Since we are only interested in disturbances travelling and growing in basic flow direction, we can restrict ourselves to values $0 < \alpha_r < 1$, $\alpha_i < 0$, and $0 < \beta < 0{\cdot}5$.

In order to evaluate the complex eigenvalues numerically we first introduce the new independent variable

$$z = \tanh y \tag{23}$$

into equation (20). Then using

$$U'' = -\tanh y \operatorname{sech}^2 y = -z(1-z^2) \tag{24}$$

we obtain

$$\frac{d\Phi}{dz} = \frac{\alpha^2 - \Phi^2}{1-z^2} - \frac{2z}{1+z-2\beta/\alpha} \tag{25}$$

and from (21) with $z_b = \pm 1$

$$\Phi(z_b) = -z_b\alpha. \tag{26}$$

Equation (25) was integrated numerically for a fixed value β starting from $z_1 = -0{\cdot}975$ to $z = 0$ which gives $\Phi_1(0)$, and starting from $z_2 = +0{\cdot}975$, which gives $\Phi_2(0)$. The initial values $\Phi(z_1)$ and $\Phi(z_2)$ were calculated by Taylor series which were expanded about $z = z_b$ up to the third-order terms. The derivatives at the boundaries z_b were evaluated from (25) using L'Hospital's rule. For three arbitrarily chosen different pairs of $\alpha = \alpha_r + i\alpha_i$ the difference

$$F(\alpha_r, \alpha_i) = \Phi_1(0) - \Phi_2(0)$$

was evaluated and improved values α were calculated from the approximated zeros of $F(\alpha_r, \alpha_i)$ by linear interpolation. This procedure was repeated until $|F|$ was sufficiently small. The computation was performed on a Zuse Z23v digital computer using a Runge–Kutta–Gill procedure with an integration step $|\Delta z| = 0{\cdot}025$.

Some functions $\Phi(z)$ are plotted in figure 1. The eigenvalues $\alpha = \alpha(\beta)$ are given

in table 1 and plotted in figure 2 together with the phase velocity $c_r = \beta_r/\alpha_r$ as a function of β_r. For comparison the curves for the timewise case after Michalke (1964) are included. We see that the curve for the spatial growth rate $(-\alpha_i)$ is only broadly similar to the curve $\alpha c_i/c_r$ which is calculated from the timewise

β	α_r	α_i	c_r
0·500	1	0	0·5
0·450	0·925761	−0·045556	0·4861
0·400	0·844361	−0·091618	0·4737
0·350	0·753444	−0·137151	0·4645
0·300	0·649548	−0·180226	0·4619
0·250	0·527421	−0·215502	0·4740
0·225	0·457728	−0·226142	0·4916
0·200	0·382625	−0·227691	0·5227
0·175	0·305869	−0·215913	0·5721
0·150	0·235039	−0·190165	0·6382
0·125	0·175861	−0·156126	0·7108
0·100	0·128087	−0·120373	0·7807
0·075	0·088817	−0·086273	0·8444
0·050	0·055452	−0·054846	0·9017
0·206692	0·403129	−0·228425	0·5127

TABLE 1

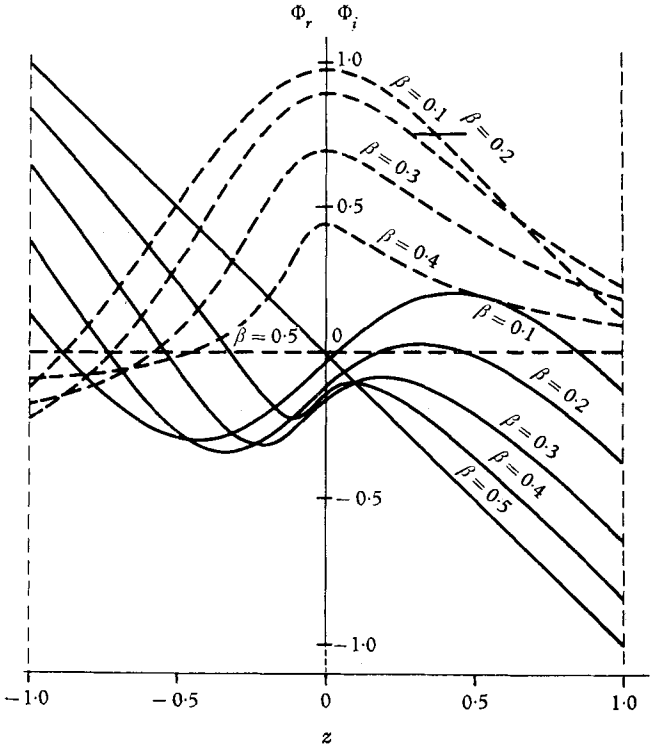

FIGURE 1. Solutions $\Phi(z)$ of equation (25) for various frequencies β: ——, $\Phi_r(z)$; – – – –, $\Phi_i(z)$.

case using the linear transformation $x = c_r t$ with $c_r = 0{\cdot}5$.† The maximum growth rate is $(-\alpha_i) = 0{\cdot}2284$ and occurs at $\beta = 0{\cdot}2067$. There the wave-number $\alpha_r = 0{\cdot}4031$ and the phase velocity $c_r = 0{\cdot}5127$. Note that the amplification is very large, since the disturbance amplitude is amplified by a factor

$$\exp(-2\pi\alpha_i/\alpha_r) \approx 35$$

within a wavelength λ.

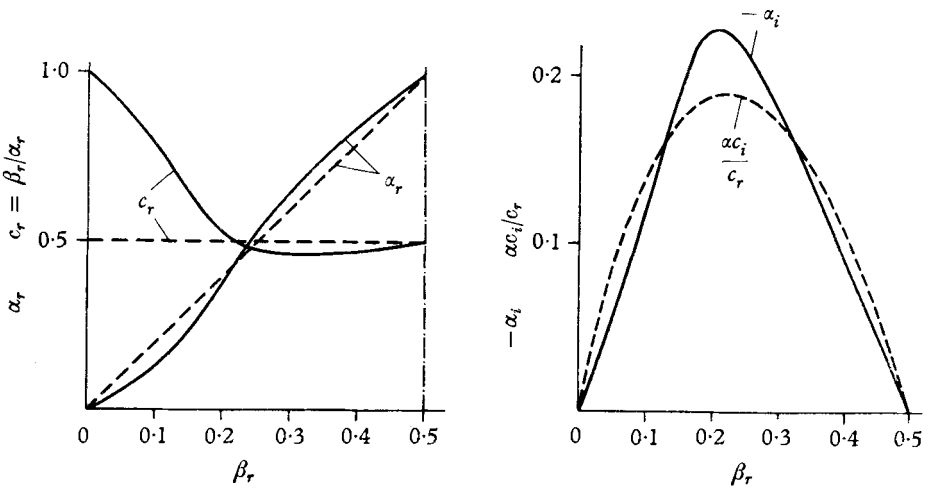

FIGURE 2. Wave-number α_r, phase velocity c_r and spatial growth rate $-\alpha_i$ (or $\alpha c_i/c_r$) *vs* frequency β_r: ——, spacewise case; – – – –, timewise case.

Furthermore, in the spacewise case the wave-number α_i is not strictly proportional to the frequency β_r as in the timewise case. Thus, contrary to the timewise case, the phase velocity c_r depends strongly on the frequency, especially for small frequencies. This behaviour, however, was observed in the experiments mentioned above.

4. Evaluation of the eigenfunctions in the spacewise case

With the computed eigenvalues we can now evaluate the eigenfunctions ϕ by integrating equation (14). Since the eigenfunctions are determined except for an arbitrary multiplicative constant alone, we normalize the initial values conveniently to

$$\phi_r(0) = 1; \quad \phi_i(0) = 0. \tag{27}$$

The initial gradient is found from (19) to be

$$\phi'(0) = \Phi(0)\,\phi(0). \tag{28}$$

Thus

$$\phi'(0) = \Phi_r(0) + i\Phi_i(0). \tag{29}$$

$\Phi(0)$, however, is known from the evaluation of the eigenvalues (§ 3). With the initial values (27) and (29) equation (14) was solved using a Runge–Kutta–Gill procedure.

In figures 3 and 4 the eigenfunctions $\phi_r(y)$ and $\phi_i(y)$ are shown for the frequencies $\beta = 0{\cdot}1$, $\beta = 0{\cdot}2$, $\beta = 0{\cdot}3$, and $\beta = 0{\cdot}4$. We see that, contrary to the timewise case, $\phi_r(y)$ and $\phi_i(y)$ are not symmetric and antisymmetric respectively.

† In the timewise case the group velocity is identical with the phase velocity, since the phase velocity does not depend on the frequency.

A comparison of the eigenfunctions for the most strongly amplified disturbance is shown in figure 5 for both the spacewise case ($\beta = 0{\cdot}2067$) and the timewise case ($\beta_r = 0{\cdot}2223$).

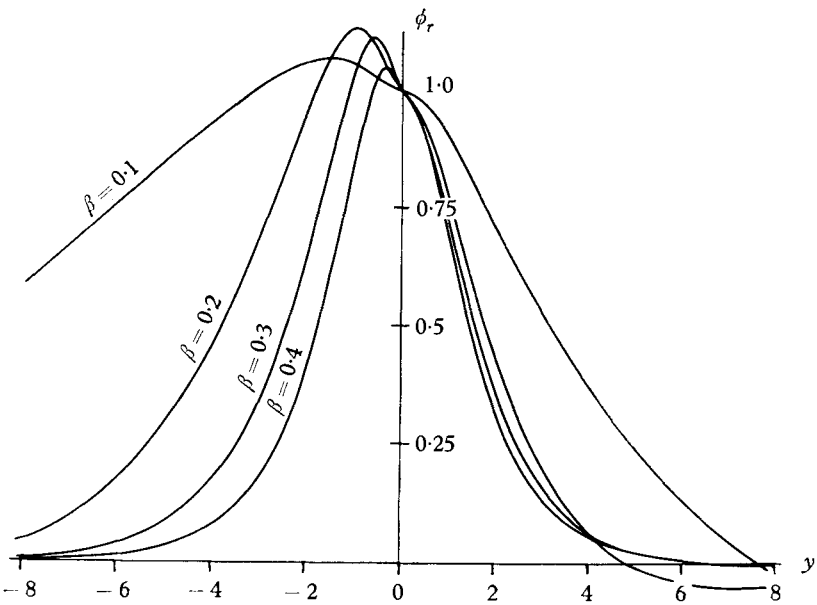

FIGURE 3. Eigenfunctions $\phi_r(y)$ of the spacewise case for various frequencies β.

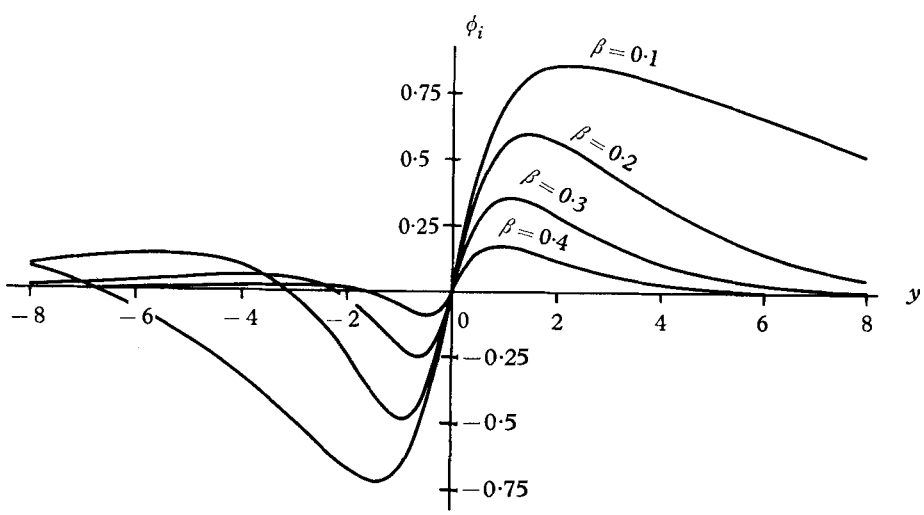

FIGURE 4. Eigenfunctions $\phi_i(y)$ of the spacewise case for various frequencies β.

The derivative $\phi'(y)$ of the eigenfunction is related to the disturbance velocity component u_1 by (11). ϕ_r' and ϕ_i' are shown in figures 6 and 7. Note that for $y < 0$ the zeros of both ϕ_r' and ϕ_i' occur at nearly the same values of y. Thus the magnitude of u_1 becomes nearly zero at this point and, therefore, we have a phase

reversal which is outside the critical layer ($y = 0$) for amplified disturbances, as was observed in the experiments mentioned above. The position of the phase reversal depends on the frequency β, as can be seen more clearly from the plot of $\Phi(z)$ in figure 1 because of the relation

$$\phi' = \Phi\phi. \tag{30}$$

For $\beta \to 0$ the phase reversal tends to $z = -1$, i.e. $y \to -\infty$, and for $\beta \to 0{\cdot}5$ to $z = y = 0$, i.e. to the position of the critical layer. This tendency has also been

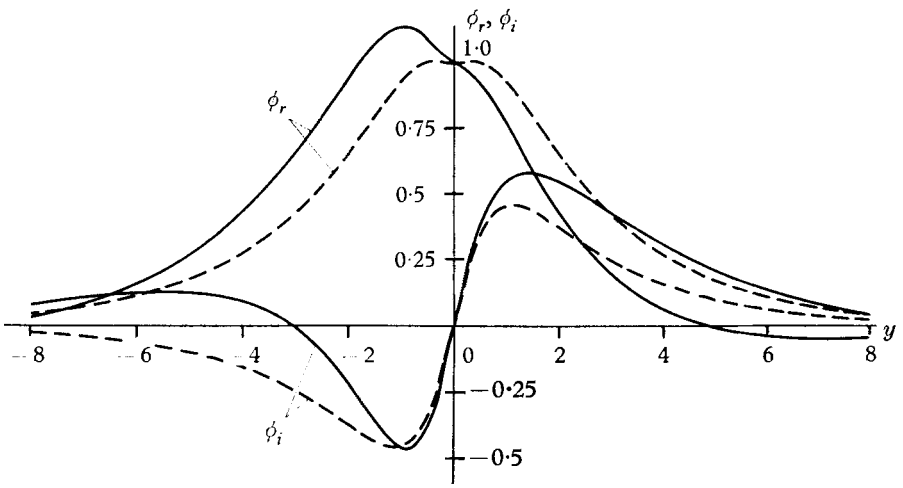

FIGURE 5. Comparison of the eigenfunctions $\phi(y)$ for the most strongly amplified disturbance: ——, spacewise case $\beta = 0{\cdot}2067$; – – – –, timewise case $\beta_r = 0{\cdot}2223$.

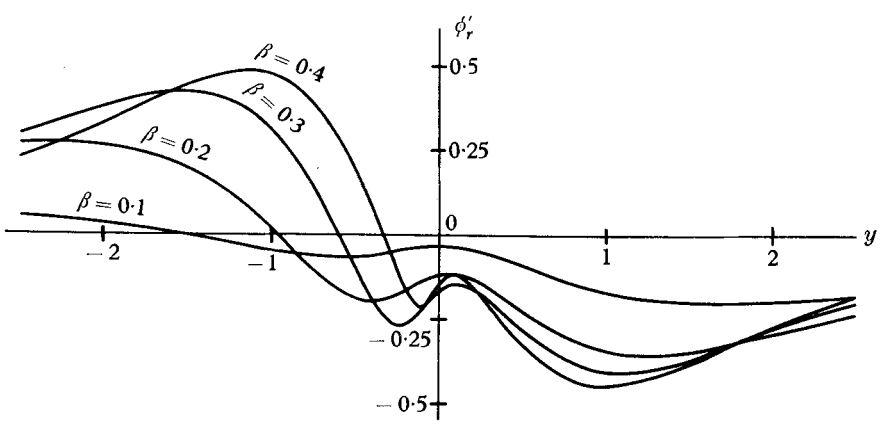

FIGURE 6. Derivative $\phi_r'(y)$ of the eigenfunction in the spacewise case for various frequencies β.

observed in experiments by Freymuth (1965). In the timewise case $|\phi'|$ is symmetric, and the zeros of ϕ_r' and ϕ_i' are apart from each other. Thus no sharp phase reversal occurs except for the neutral disturbance.

Thus it is obvious that the theory of spatially growing disturbances includes many essential features of the instability properties of shear layers which are

known from experiment. This is not surprising from a physical point of view, since in the experiments the disturbances in fact grow in space and not in time. Thus we may conclude that the spacewise theory gives a better description of the shear-layer instability than the timewise case. But the verification of this statement can only be made by comparing the results of the experimental investigations with those of both theories. This was performed by Freymuth (1965) and is described briefly in the appendix.

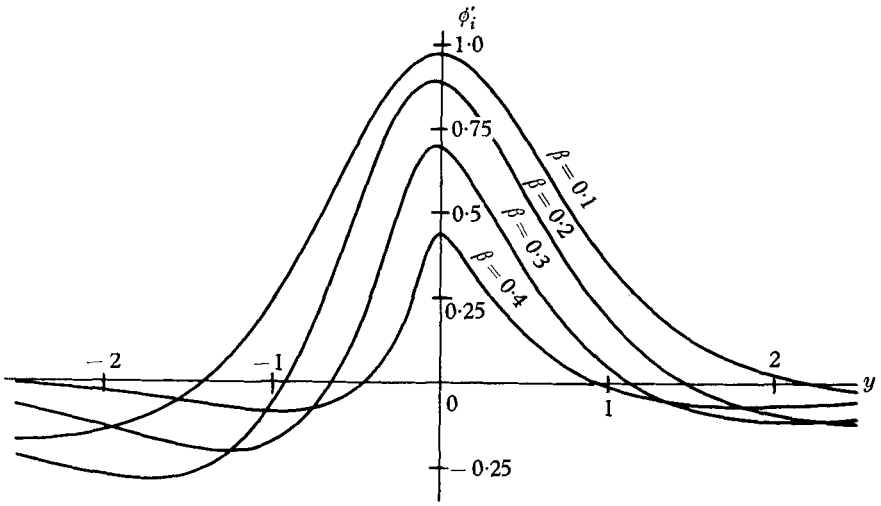

FIGURE 7. Derivative $\phi_i'(y)$ of the eigenfunction in the spacewise case for various frequencies β.

5. The vorticity distribution in the disturbed shear layer

Let us now discuss some further properties of the disturbed shear layer. With the computed eigenfunctions we can evaluate the streamlines, the velocity field and the vorticity distribution of the disturbed flow. It was shown by Michalke (1964) that the streamlines are not particularly significant. Therefore we shall first calculate the vorticity distribution.

The distribution of the vorticity $\Omega_0(y)$ of the basic flow is given by (5),

$$\Omega_0(y) = -0{\cdot}5\,\mathrm{sech}^2 y, \tag{31}$$

and the disturbance vorticity $\Omega_1(x, y, t)$ is defined by (12). The complex amplitude function $\omega(y)$ was computed together with the eigenfunctions (§ 4) using (13) from the relation

$$\omega(y) = -\{U''/(U-\beta/\alpha)\}\phi. \tag{32}$$

Figures 8 and 9 show $\omega_r(y)$ and $\omega_i(y)$ for the frequencies $\beta = 0{\cdot}1$, $\beta = 0{\cdot}2$, $\beta = 0{\cdot}3$ and $\beta = 0{\cdot}4$. It is evident from (32) that for $\alpha_i \neq 0$ the value of $\omega_r(0)$ is zero because $U''(0) = 0$, but for the neutral case ($\beta = 0{\cdot}5$) where $\omega_r(y) = 2\,\mathrm{sech}^3 y$ we have $\omega_r(0) = 2$. Thus analogous to the timewise case there is no uniform convergence of $\omega_r(0)$ as β tends to the neutral value 0·5. According to (7), (12), and (31) the total vorticity distribution is given by

$$\Omega(x, y, t) = -0{\cdot}5\,\mathrm{sech}^2 y + \epsilon\, e^{-\alpha_i x}\{\omega_r(y)\cos(\alpha_r x - \beta t) - \omega_i(y)\sin(\alpha_r x - \beta t)\} \tag{33}$$

and is periodic in time.

For a fixed time t the lines of constant vorticity can be evaluated by using an iteration process. They were computed for the most strongly amplified disturbance ($\beta = 0{\cdot}2067$) for $t = T = 2\pi/\beta$ and for $t = 1{\cdot}5T$. The disturbance magnitude was chosen very small, namely $\epsilon = 0{\cdot}0005$. The results are plotted in figure 10.

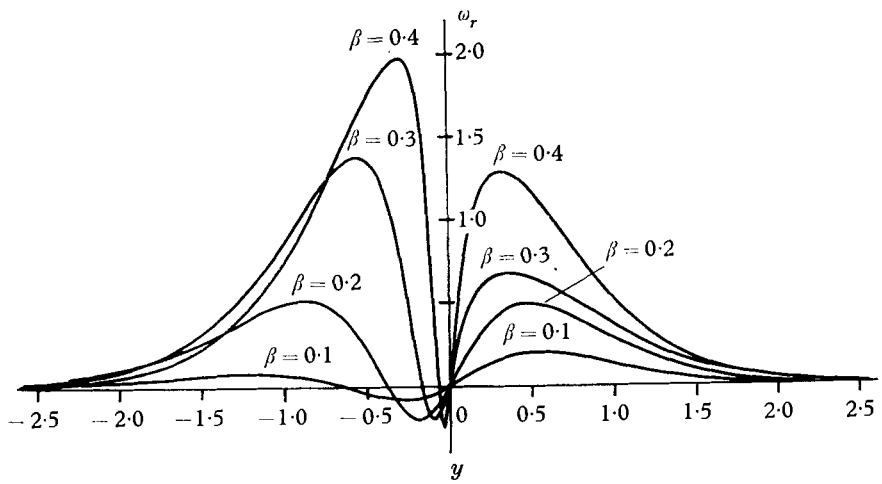

FIGURE 8. Vorticity amplitude $\omega_r(y)$ of the spacewise case for various frequencies β.

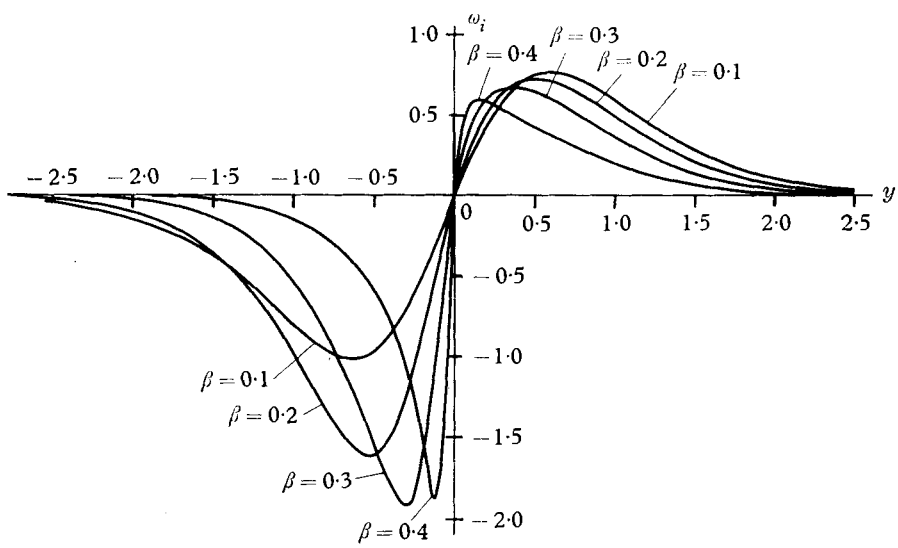

FIGURE 9. Vorticity amplitude $\omega_i(y)$ of the spacewise case for various frequencies β.

Note that the length scale in the y-direction is enlarged by a factor 5 in order to show the phenomenon more clearly. We see that the lines of constant vorticity, which are straight lines parallel to the x-axis for the undisturbed flow ($\epsilon = 0$), are displaced sinuously by the disturbance. With increasing local disturbance magnitude

$$\bar{\epsilon}(x) = \epsilon e^{-\alpha_i x}, \tag{34}$$

the vorticity is redistributed causing two peaks of vorticity within a disturbance wavelength λ, one for $y < 0$ and one for $y > 0$, the latter being smaller than the

former at the same x. Because of their mutual induction these peaks of vorticity will superimpose a rotational motion on the basic flow showing quite clearly the mechanism of instability.

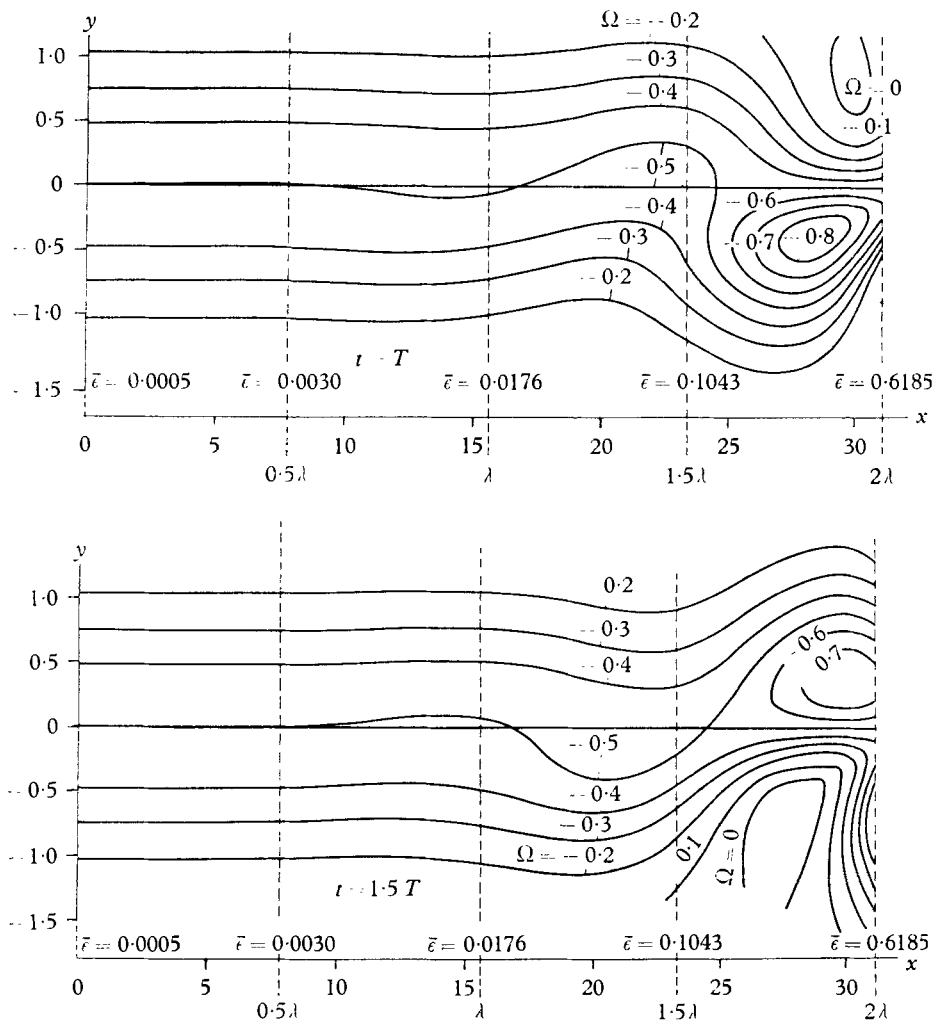

FIGURE 10. Lines of constant vorticity of the disturbed hyperbolic-tangent velocity profile in the spacewise case for the frequency $\beta = 0{\cdot}2067$ of maximum amplification at two different times t; disturbance magnitude $\epsilon = 0{\cdot}0005$ (inviscid linearized theory).

6. The streaklines of the disturbed flow

Since the velocity distribution of the disturbed flow according to the inviscid linearized theory is known, we can also calculate the motion of any particle of the flow. It may be of special interest to study the spatial development of the disturbed shear layer, which can be done by means of the streakline pattern. A streakline is defined as a line connecting the positions of particles at a fixed time which went through the same point of the flow field at different times. In experiments the streaklines or their envelopes can be visualized by introducing

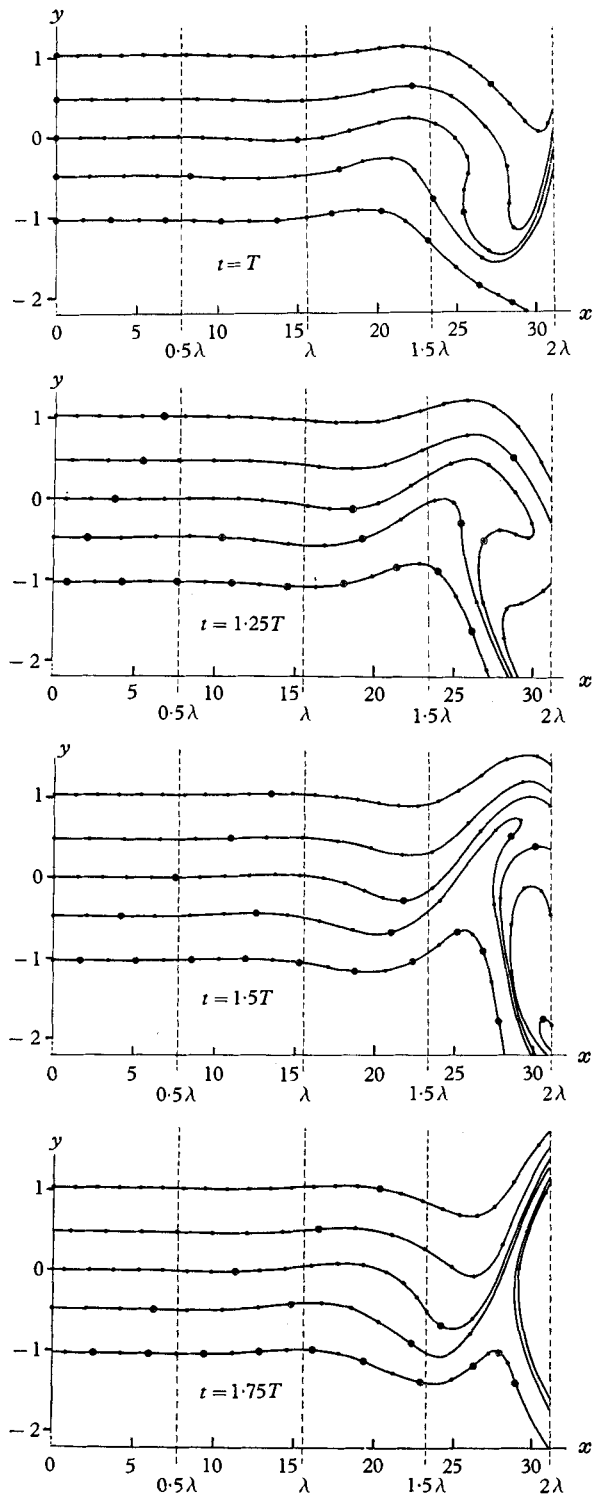

FIGURE 11. Streakline pattern of the disturbed hyperbolic-tangent velocity profile in the spacewise case for the frequency $\beta = 0{\cdot}2067$ at four different times t; disturbance magnitude $\epsilon = 0{\cdot}0005$ (inviscid linearized theory).

smoke or dye into the flow. The velocity field of the disturbed shear layer is given by (6). Using (11) and (12) we obtain

$$\left.\begin{aligned} u(x,y,t) &= 0{\cdot}5[1+\tanh y]+\epsilon\, e^{-\alpha_i x}\{\phi_r'(y)\cos(\alpha_r x-\beta t)-\phi_i'(y)\sin(\alpha_r x-\beta t)\},\\ v(x,y,t) &= \epsilon\, e^{-\alpha_i x}\{[\alpha_i\phi_r(y)+\alpha_r\phi_i(y)]\cos(\alpha_r x-\beta t)\\ &\qquad +[\alpha_r\phi_r(y)-\alpha_i\phi_i(y)]\sin(\alpha_r x-\beta t)\}. \end{aligned}\right\} \quad (35)$$

The motion of a particle is governed by the differential equation of the path lines

$$dx/dt = u(x(t),y(t),t), \quad dy/dt = v(x(t),y(t),t), \quad (36)$$

where the right-hand sides are given by (35). $x(t)$ and $y(t)$ denote the position of a particle at the time t. In order to determine a pathline the appropriate initial conditions are

$$x(t_0) = x_0, \quad y(t_0) = y_0. \quad (37)$$

For the neutral disturbance of the tanh velocity profile the streakline pattern was computed by Hama (1962).

In our calculation x_0 was chosen to be zero, and $\epsilon = 0{\cdot}0005$. For the most strongly amplified disturbance ($\beta = 0{\cdot}2067$) the pathlines of particles were calculated numerically using a Runge–Kutta–Gill procedure starting from $x_0 = 0$ and $y_0 = 0, \pm 0{\cdot}4812117, \pm 1{\cdot}0317184$. These points were chosen because there the undisturbed vorticity $\Omega_0 = -0{\cdot}5, -0{\cdot}4, -0{\cdot}2$ respectively. In order to plot each streakline for a fixed time with sufficient accuracy one has to compute pathlines for various initial times t_0 which can be restricted to the interval $0 \leqslant t_0 \leqslant T$ because of the periodicity of the flow with respect to time. In figure 11 the shape of the streaklines is shown for the times $t = T$; $1{\cdot}25T$; $1{\cdot}5T$; $1{\cdot}75T$. The positions of particles started with constant time delay for each streakline are marked by points. Furthermore, particles starting at $t_0 = nT$ ($n = 0, \pm 1, \pm 2, \ldots$) from its initial position are marked by a circle.

We see that particles starting originally in the region of higher velocity ($y > 0$) move to the region of lower velocity ($y < 0$), where they are retarded so that other particles started later can pass by and vice versa. Thus the streaklines show a tendency to roll up in a complicated manner with a coincidental folding of the lines. The shape of the disturbed shear layer found here is similar to that observed by means of the smoke technique in jet boundary layers (cf. Michalke & Wille 1965; Freymuth 1965).

7. Estimate of the validity of the linearized theory

Both from the vorticity distribution (figure 10) and from the streaklines (figure 11) we see that the local disturbance magnitude (34) grows rapidly and becomes, for instance, $\bar{\epsilon} = 0{\cdot}6185$ at $x = 2\lambda$. Therefore the question arises as to what extent is the linearized theory valid. As mentioned in § 2 the linearization of equation (8) is surely justified, if both conditions (9) are satisfied. We shall now examine these conditions. The first one gives with (11) and (12)

$$U(y) \gg \epsilon\, e^{-\alpha_i x}|\phi'| = \bar{\epsilon}\,|\phi'|. \quad (38)$$

Since $U(y)$ tends to 1 for $y \to \infty$ and we have $|\phi'| < 1$ according to figures 6 and 7, the condition (38) is certainly satisfied for $y > 0$, if the local disturbance magni-

tude $\bar{\epsilon}$ is sufficiently small. On the other hand, for $y \to -\infty$ the behaviour of our basic flow is $U(y) \sim e^{2y}$, but that of the disturbance is $|\phi'| \sim e^{\alpha_r y}$. Since we have $\alpha_r \leqslant 1 < 2$, the basic velocity vanishes more rapidly for $y \to -\infty$ than the disturbance velocity and, however small $\bar{\epsilon}$ may be, both velocities become comparable in a certain region. Yet this may occur far outside the shear layer, and therefore this violation of condition (38) may be negligible. From the second condition of (9) we obtain with (12)

$$|U''| \gg \epsilon e^{-\alpha_i x} |\omega'| = \bar{\epsilon} |\omega'|. \tag{39}$$

Since U''—see (24)—becomes zero at the critical layer $y = 0$, this condition is violated unless $|\omega'|$ also vanishes at this point. From (32) it follows that

$$|\omega'| = \left| \left(\frac{U''}{U - \beta/\alpha} \right)' \phi + \left(\frac{U''}{U - \beta/\alpha} \right) \phi' \right|. \tag{40}$$

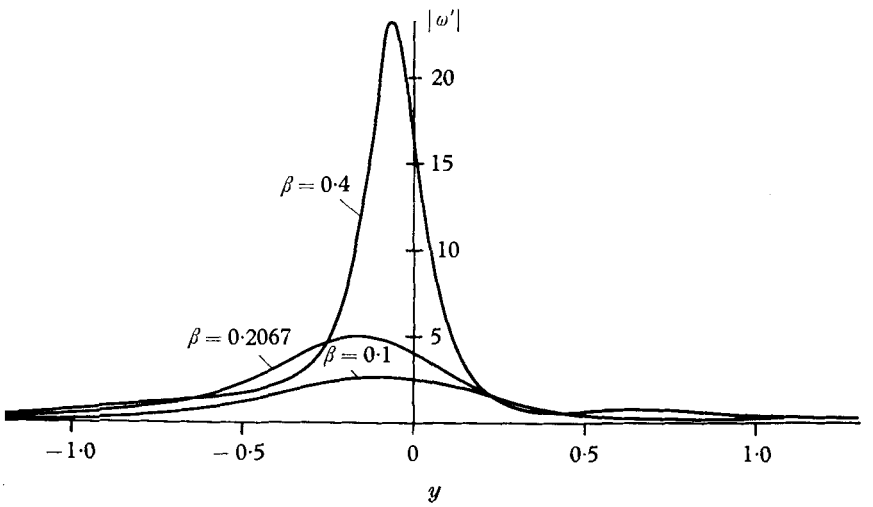

FIGURE 12. $|\omega'|$ as a function of y for various frequencies β in the spacewise case.

This function was calculated and is plotted in figure 12 for $\beta = 0{\cdot}1$, $\beta = 0{\cdot}4$, and for the most strongly amplified disturbance with $\beta = 0{\cdot}2067$. It is evident that for amplified disturbances $|\omega'(0)|$ is unequal to zero, and its value increases strongly, if β tends to 0·5, i.e. if we approach the neutral case. Thus it follows that in the neighbourhood of the critical layer the non-linear terms of (8) become important for amplified disturbances even though the local disturbance magnitude $\bar{\epsilon}$ is small. This was stated by Lin (1958). Note that for $\beta = 0{\cdot}1$ we have $\max |\omega'| = 2{\cdot}6$, but $\max |\omega'| = 23{\cdot}3$ for $\beta = 0{\cdot}4$, although their spatial growth rates $(-\alpha_i)$ have nearly the same values. Therefore the error due to the linearization of equation (8) for $\beta = 0{\cdot}4$ might also be one order of magnitude larger than for $\beta = 0{\cdot}1$.

Let us now estimate the total error made by the linearization of the equation of motion. Formally we can write the disturbance equation (8) as an integral equation

$$\epsilon \Omega_1 = -\int \left\{ \epsilon \left[U \frac{\partial \Omega_1}{\partial x} - U'' v_1 \right] + R_\Omega \right\} dt, \tag{41}$$

where the quantity R_Ω is given by

$$R_\Omega = \epsilon^2[u_1\,\partial\Omega_1/\partial x + v_1\,\partial\Omega_1/\partial y]. \tag{42}$$

If we now use the solution of the linearized equation (10), we get

$$\epsilon\,\Omega_1 = \int\left[\epsilon\frac{\partial\Omega_1}{\partial t} - R_\Omega\right]dt. \tag{43}$$

This equation is only satisfied if the residual term R_Ω can be neglected compared with $\epsilon\,\partial\Omega_1/\partial t$. Now, we have

$$\epsilon\,\partial\Omega_1/\partial t = O(\bar{\epsilon}\beta|\omega|) \tag{44}$$

and

$$|R_\Omega| < \epsilon^2[\,|u_1\,\partial\Omega_1/\partial x| + |v_1\,\partial\Omega_1/\partial y|\,], \tag{45}$$

or using (11), (12) and (34) we find

$$|R_\Omega| < \bar{\epsilon}^2\tilde{R}_\Omega(y), \tag{46}$$

with

$$\tilde{R}_\Omega = |\alpha|\,\{|\phi'|\,|\omega| + |\phi|\,|\omega'|\}. \tag{47}$$

Analogously we obtain a relation similar to (43) from the Euler equation of motion for the velocity component u_1

$$\epsilon u_1 = \int[\epsilon\,\partial u_1/\partial t - R_u]\,dt, \tag{48}$$

where

$$\epsilon\,\partial u_1/\partial t = O(\bar{\epsilon}\beta|\phi'|) \tag{49}$$

and

$$|R_u| = \epsilon^2|u_1\,\partial u_1/\partial x + v_1\,\partial u_1/\partial y| < \bar{\epsilon}^2\tilde{R}_u, \tag{50}$$

with

$$\tilde{R}_u = |\alpha|\,\{|\phi'|^2 + |\alpha|^2|\phi|^2 + |\phi|\,|\omega|\}. \tag{51}$$

For the velocity component v_1 the relation becomes

$$\epsilon v_1 = \int[\epsilon\,\partial v_1/\partial t - R_v]\,dt, \tag{52}$$

where

$$\epsilon\,\partial v_1/\partial t = O(\bar{\epsilon}\beta|\alpha|\,|\phi|) \tag{53}$$

and

$$|R_v| = \epsilon^2|u_1\,\partial v_1/\partial x + v_1\,\partial v_1/\partial y| < \bar{\epsilon}^2\tilde{R}_v, \tag{54}$$

with

$$\tilde{R}_v = 2|\alpha|^2|\phi|\,|\phi'|. \tag{55}$$

It is quite clear that the residual terms depend (i) on the local disturbance magnitude $\bar{\epsilon}$ and (ii) on y and implicitly on β. If a fixed local disturbance magnitude $\bar{\epsilon}$ is assumed, the validity of the linearization will only depend on the terms $\tilde{R}_v$, $\tilde{R}_u$ and $\tilde{R}_\Omega$. They are plotted in the figures 13–15 for $\beta = 0{\cdot}1$, $0{\cdot}2067$ and $0{\cdot}4$. The ratios between the maximum values of $\tilde{R}_v$, $\tilde{R}_u$ and $\tilde{R}_\Omega$ are

for $\beta = 0{\cdot}1$

$$\max(\tilde{R}_v) : \max(\tilde{R}_u) : \max(\tilde{R}_\Omega) = 0{\cdot}06 : 0{\cdot}29 : 0{\cdot}52 \approx 1 : 5 : 9;$$

for $\beta = 0{\cdot}2067$

$$\max(\tilde{R}_v) : \max(\tilde{R}_u) : \max(\tilde{R}_\Omega) = 0{\cdot}39 : 1{\cdot}15 : 2{\cdot}74 \approx 1 : 3 : 7;$$

for $\beta = 0{\cdot}4$

$$\max(\tilde{R}_v) : \max(\tilde{R}_u) : \max(\tilde{R}_\Omega) = 0{\cdot}68 : 2{\cdot}81 : 20{\cdot}20 \approx 1 : 4 : 30.$$

It follows that for fixed frequency the residual terms connected with the velocity components v_1 and u_1 are smaller than those connected with the vorticity Ω_1 and

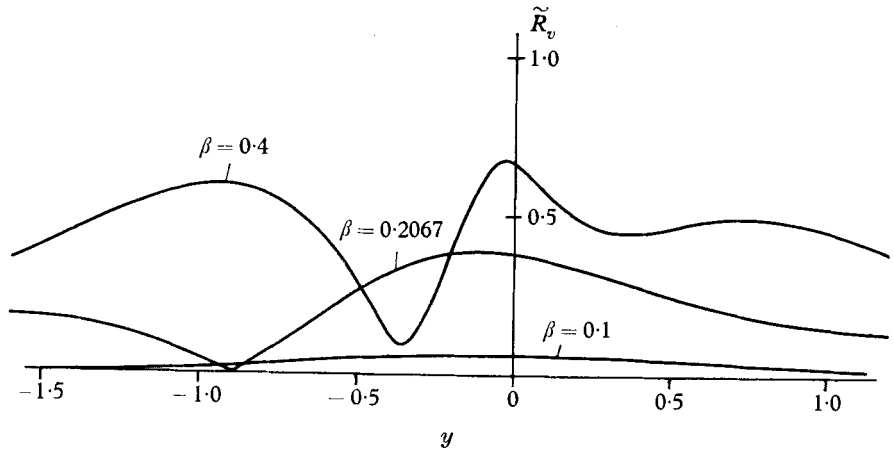

FIGURE 13. $\tilde{R}_v$ as a function of y for various frequencies β in the spacewise case.

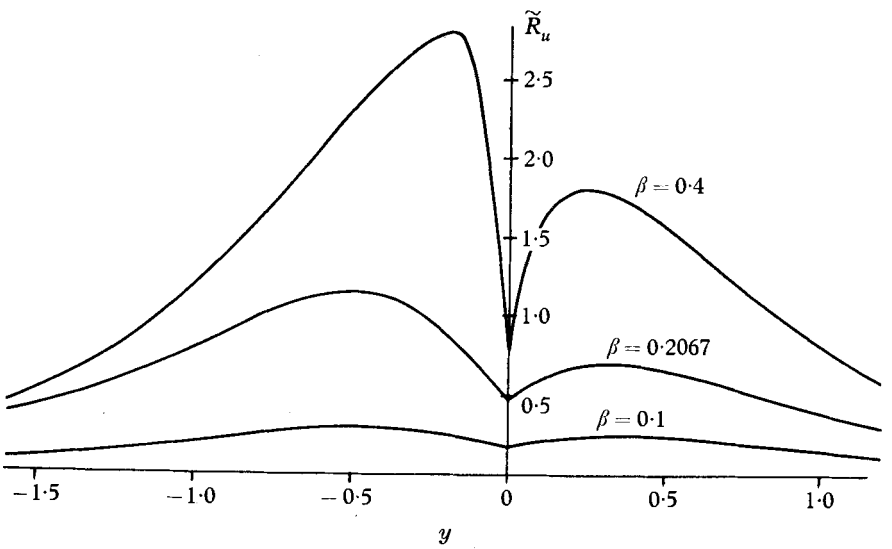

FIGURE 14. $\tilde{R}_u$ as a function of y for various frequencies β in the spacewise case.

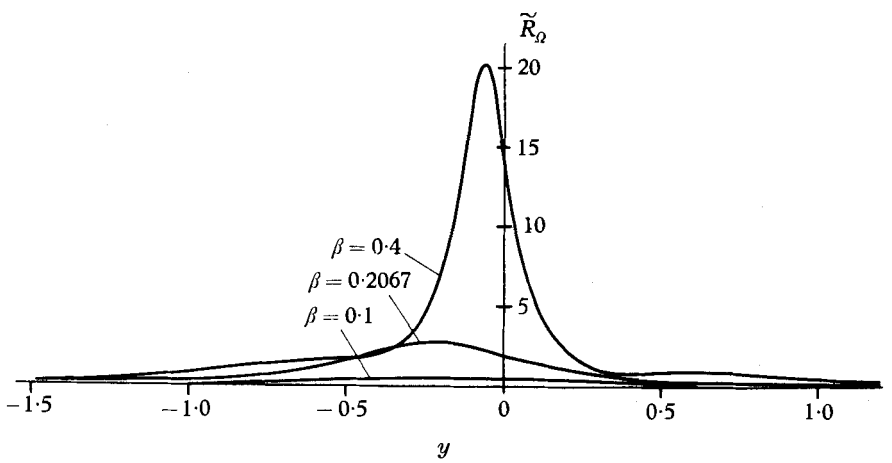

FIGURE 15. $\tilde{R}_\Omega$ as a function of y for various frequencies β in the spacewise case.

that, furthermore, the residual terms for small frequencies are smaller than those for higher frequencies.

Thus we may conclude that the region of validity of the linearized equation should be larger for the velocity distribution than for the vorticity distribution and larger for small frequencies than for higher frequencies. Nevertheless, from these estimates an exact bound for the validity of the linearized equations cannot be derived. But from the physical meaning of the Helmholtz equation (1) a good criterion can be obtained as was shown by Michalke (1965). From the non-linear equation (1) it follows that, if a particle of the flow is moving along its pathline, its vorticity remains constant for all times. Suppose now that the vorticity is constant in time at the point (x_0, y_0) where the particles forming a streakline start; then it follows that the streakline has to be identical with a line of constant vorticity for all times. Furthermore, if the vorticity distribution for $x \to -\infty$ (where the disturbance vanishes) has an extremum, it follows from the Helmholtz equation that this value cannot be exceeded at any time or any point of the flow.

Let us now examine the results of §§ 5 and 6 by this means. At $x = x_0 = 0$ the variation $\Delta\Omega$ in time of the basic vorticity $\Omega_0(y)$ caused by the disturbance vorticity is smaller than

$$|\Delta\Omega| \leqslant \epsilon|\Omega_1| = \epsilon|\omega|. \tag{56}$$

For the most strongly amplified disturbance the magnitude of ω is $|\omega| < 1{\cdot}7$. Then for the disturbance magnitude $\epsilon = 0{\cdot}0005$ we find $|\Delta\Omega| < 0{\cdot}00085$, which should be negligible compared with $\Omega_0(y)$. Thus the assumption that for all particles starting at $x_0 = 0$ the corresponding vorticity is $\Omega_0(y)$ and that the extremum vorticity is $\Omega_0(0) = -0{\cdot}5$ is justified.† The initial values y_0 of the five computed streaklines were chosen so that they would be identical with the lines of constant vorticity $\Omega = -0{\cdot}2$; $-0{\cdot}4$; and $-0{\cdot}5$ respectively as described above. Figure 16 shows the comparison of the streaklines and the corresponding lines of constant vorticity for $t = T$ and $t = 1{\cdot}5T$. We see that outside the critical layer $y = 0$ the agreement is good up to $x = 1{\cdot}5\lambda$, where differences appear. Therefore we may conclude that in these regions of the flow the linearized theory suffices. Yet in the neighbourhood of the critical layer $y = 0$ we find disagreement even for small values of x as expected. The line of initially extremum vorticity $\Omega = -0{\cdot}5$ is split into two lines with a region of higher vorticity between them. This is not compatible with the non-linear equations. Yet we know from the estimates above that the error due to the linearization is expected to be smaller in the velocity field than in the vorticity field. Since for the calculation of the streaklines only the velocity field due to the linearized theory is used, it may therefore be supposed that the streaklines give a more correct impression of the vorticity distribution due to the non-linear theory than the lines of constant vorticity calculated by means of the linearized theory.

The results obtained by Hama (1962) for the neutral disturbance of the hyperbolic-tangent velocity profile are more difficult to interpret, since there the calculated streaklines certainly do not correspond to lines of constant vorticity,

† For comparison the variation $\Delta\Omega$ in time used by Hama (1962) for his computation of the streaklines in the neutral case was $|\Delta\Omega| \leqslant 0{\cdot}04$, $0{\cdot}08$, $0{\cdot}2$, which seems to be insufficiently small in relation to the extremum basic vorticity used, $\Omega_0(0) = -1$.

because of the relatively large vorticity variation $\Delta\Omega$ of the particles at the starting-points as mentioned above. But the principal statement of Hama that there is no vorticity concentration in the disturbed flow is not strictly correct, since even in the neutral case a certain vorticity concentration exists in the disturbed flow as was shown by Michalke (1964).

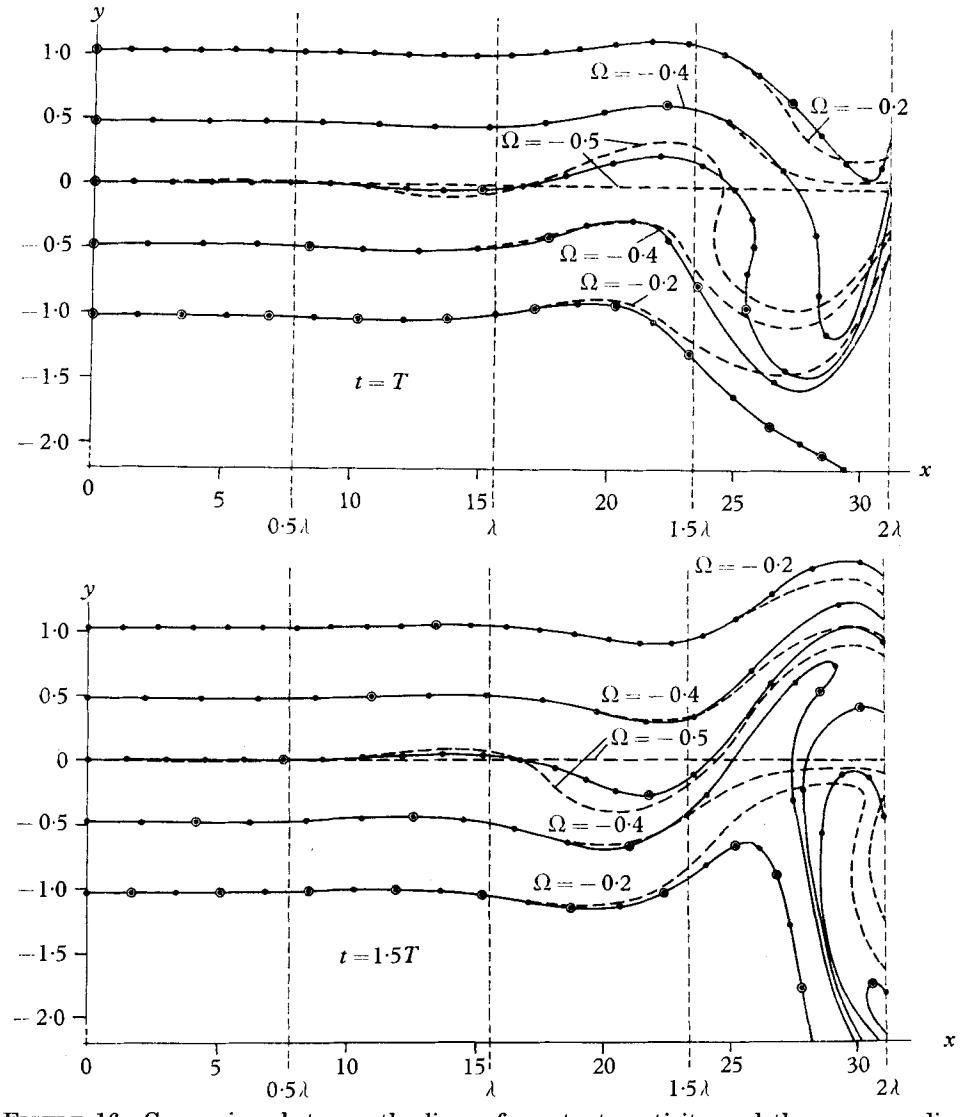

FIGURE 16. Comparison between the lines of constant vorticity and the corresponding streaklines for the spacewise case according to the inviscid linearized theory at two different times t. Disturbance frequency $\beta = 0{\cdot}2067$; disturbance magnitude $\epsilon = 0{\cdot}0005$.

Finally, we can conclude from the above considerations of the non-linear equation that in shear layers which can be treated as inviscid the streakline pattern visualized by smoke gives an impression of the vorticity distribution. But it is known from many authors, cf. Michalke & Wehrmann (1964) and Wille

(1963), that discrete concentrations of smoke were observed in disturbed free boundary layers. Freymuth (1965) has shown also that in these regions of the free boundary layer the flow is not noticeably affected by viscosity and can be treated as inviscid, if the Reynolds number is large. Thus it follows that these concentrations of smoke must be identical with concentrations of vorticity which can be interpreted as discrete vortices. This may be a confirmation that a disturbed free boundary layer rolls up into discrete vortices for large Reynolds numbers.

Appendix

Comparison of experimental results with those of the spatial and temporal theory

Freymuth (1965) compared experimental results obtained from disturbed axisymmetric and plane jet boundary layers with those from the inviscid linearized stability theory of both the spacewise and timewise case. He found that from a distance $x = 10\Theta_m$ downstream of the nozzles from which the jets were produced the measured undisturbed velocity profiles can be expressed approximately by

$$U(y)/U_0 = 0{\cdot}5[1 + \tanh(0{\cdot}5y/\Theta_m)],$$

where Θ_m is the momentum thickness of the free boundary layer. Since these profiles depend only implicitly on the Reynolds number through change in Θ_m, this dependence on the Reynolds number can be eliminated by chosing Θ_m as a characteristic length scale. The Reynolds number R_{Θ_m} based on the maximum velocity U_0 of the shear layer and the momentum boundary-layer thickness Θ_m was varied in the interval $61 \leqslant R_{\Theta_m} \leqslant 334$. It was confirmed by Freymuth that by chosing Θ_m as a length scale the instability properties of the disturbed shear layer also were independent of the Reynolds number in this interval.

Freymuth excited artificial disturbances of various frequencies f in the jet boundary layer by a loudspeaker. Then he measured the wavelength λ of the disturbances and the distribution of the velocity fluctuations by means of a hot-wire technique. From the wavelengths λ Freymuth obtained the wavenumbers α_r and plotted these in dimensionless form as a function of the dimensionless frequency, i.e. Strouhal number $f\Theta_m/U_0$, including both the corresponding theoretical curves of the timewise and spacewise case. We see from figure 17 that for $f\Theta_m/U_0 < 0{\cdot}02$ the measured values agree with the spacewise rather than the timewise case. This can also be seen by considering the phase velocity c_r/U_0 of the disturbance, which is plotted in figure 18.

Furthermore, Freymuth measured the fundamental component of the velocity fluctuation which is equivalent to the fluctuation component in the basic flow direction ($u' = |\epsilon u_1|$). In figure 19 the measured distribution of $|\phi'| \sim u'$ is compared with both theoretical curves for a Strouhal number $f\Theta_m/U_0 = 0{\cdot}008$. Here also a better agreement is found with the spacewise theory. From the growth of the maximum peak of the velocity fluctuations u' in the basic flow direction x Freymuth evaluated the growth rates ($-\alpha_i \Theta_m$) and plotted these as a function of the Strouhal number $f\Theta_m/U_0$. It is evident from figure 20 that for

$f\Theta_m/U_0 \leqslant 0{\cdot}01$ the growth rates obtained experimentally agree with the spacewise theory. For $f\Theta_m/U_0 > 0{\cdot}01$ the results are doubtful, because exponentially growing disturbances exist only for small values x in the basic flow direction. Freymuth found that, in agreement with theory (§ 7), for increasing frequency

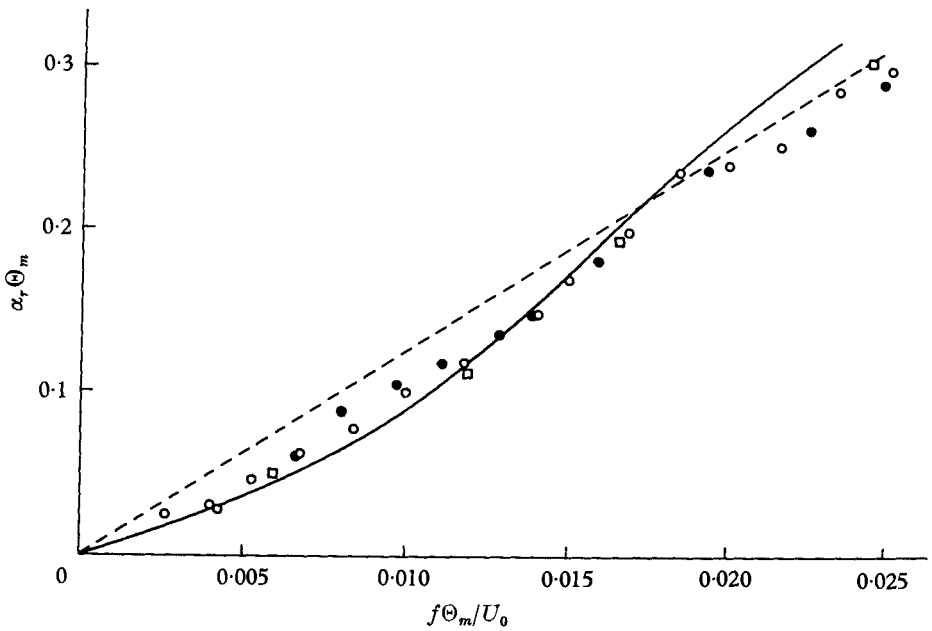

FIGURE 17. Non-dimensional wave-number *vs* Strouhal number measured in the free boundary layer of an axisymmetric jet (○, $U_0 = 8$ m/sec; ●, $U_0 = 4$ m/sec) and of a plane jet (□, $U_0 = 8$ m/sec) compared with the spacewise theory (——) and the timewise theory (– – – – –) after Freymuth.

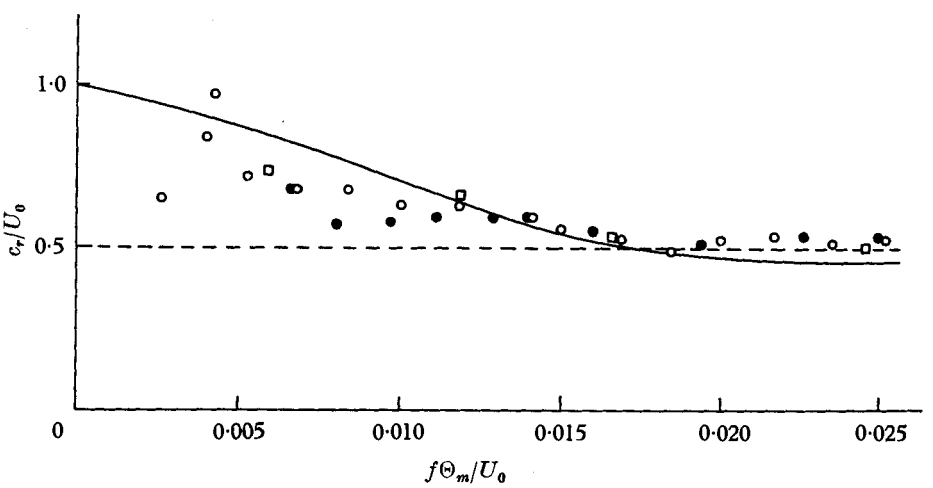

FIGURE 18. Non-dimensional phase velocity *vs* Strouhal number in the free boundary layer of an axisymmetric jet (○, $U_0 = 8$ m/sec; ●, $U_0 = 4$ m/sec) and of a plane jet (□, $U_0 = 8$ m/sec) compared with the spacewise theory (——) and the timewise theory (– – – – –) after Freymuth.

the influence of the non-linearity becomes remarkable even for small disturbances. It may be noticed that Freymuth was unable to excite disturbances artificially for frequencies $0{\cdot}0250 \leqslant f\Theta_m/U_0 \leqslant 0{\cdot}0398$, the higher of which limits is equivalent to the neutral disturbance.

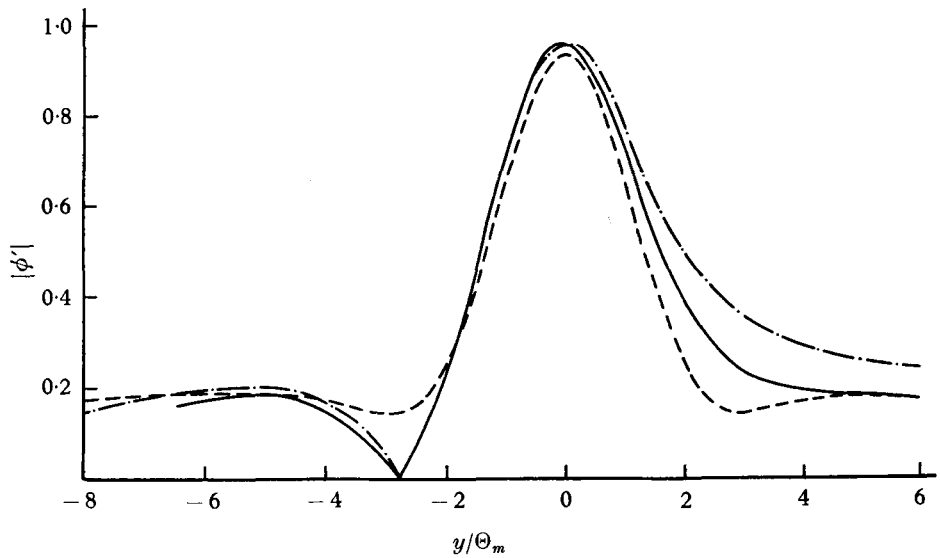

FIGURE 19. Amplitude distribution $|\phi'|$ of the velocity fluctuation in basic flow direction measured in the axisymmetric jet boundary layer (—·—·—) for $f\Theta_m/U_0 = 0{\cdot}008$ with the corresponding distribution due to the spacewise theory (——) and the timewise theory (– – – –) after Freymuth.

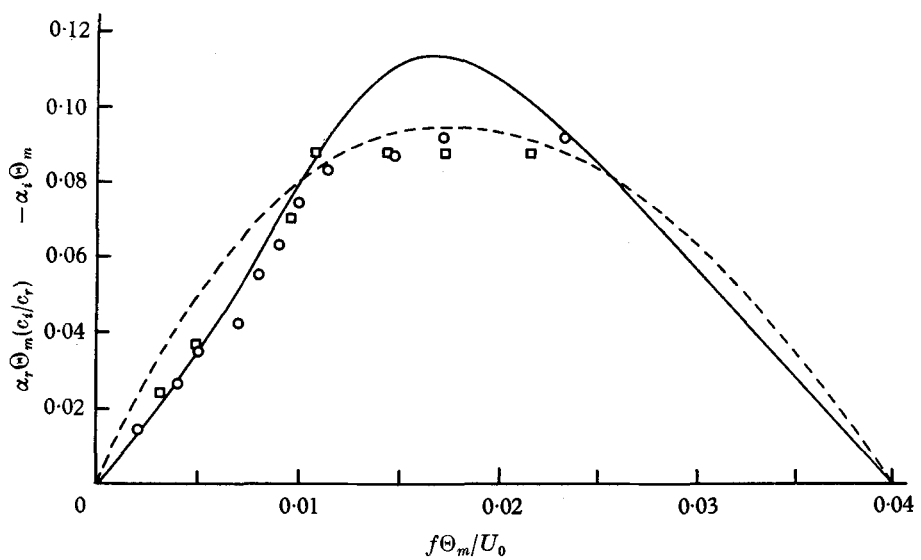

FIGURE 20. Spatial growth rates measured in the free boundary layer of an axisymmetric jet (○, U_0 = 8 m/sec) and of a plane jet (□, U_0 = 8 m/sec) compared with those of the spacewise theory (——) and the timewise theory (– – – –) after Freymuth.

Nevertheless from these experimental results we can conclude with Freymuth that, at least for small frequencies, the growth of disturbances in a free boundary layer can more precisely be described by the stability theory of spatially growing disturbances.

This investigation was made at the Institut für Turbulenzforschung of the Deutsche Versuchsanstalt für Luft- und Raumfahrt e.V. at Berlin. The author wishes to express his gratitude to Prof. Dr.-Ing. R. Wille, the Director of the Institut, and to Dipl.-Ing. P. Freymuth for many stimulating discussions. The author is also much indebted to the Deutsche Forschungsgemeinschaft, Bad Godesberg, which kindly gave financial support for the numerical computations.

REFERENCES

Betchov, R. & Szewczyk, A. 1963 *Phys. Fluids*, **6**, 1391–6.

Esch, R. E. 1957 *J. Fluid Mech.* **3**, 289–303.

Fabian, H. 1960 *Deutsche Versuchsanstalt f. Luftfahrt, Porz-Wahn, DVL-Rep.* no. 122.

Freymuth, P. 1965 Diss. Technische Universität Berlin. (To be published.)

Gaster, M. 1962 *J. Fluid Mech.* **14**, 222–4.

Gaster, M. 1965 *Progr. Aero. Sci.* **6**, 251–70.

Gill, A. E. 1965 *J. Fluid Mech.* **21**, 145–72.

Hama, F. R. 1962 *Phys. Fluids*, **5**, 644–50.

Leite, R. J. 1956 *Univ. Michigan Engng Coll. Rep.* IP-188.

Lessen, M. 1950 *Nat. Adv. Comm. Aero., Wash., Tech. Rep.* no. 979.

Lin, C. C. 1955 *The Theory of Hydrodynamic Stability.* Cambridge University Press.

Lin, C. C. 1958 *Boundary Layer Research* (ed. H. Görtler), pp. 144–57. Berlin–Göttingen–Heidelberg: Springer-Verlag.

Michalke, A. 1964 *J. Fluid Mech.* **19**, 543–56.

Michalke, A. 1965 *J. Fluid Mech.* **22**, 371–83.

Michalke, A. & Schade, H. 1963 *Ing. Arch.* **33**, 1–23.

Michalke, A. & Wehrmann, O. 1964 *Proc. Intern. Counc. Aero. Sci. 3rd Congr., Stockholm*, 1962, pp. 773–85.

Michalke, A. & Wille, R. 1965 *Proc. 11th Intern. Congr. Appl. Mech., Munich*, 1964.

Rayleigh, Lord 1880 *Sci. Papers*, **1**, pp. 474–87. Cambridge University Press.

Sato, H. 1956 *J. Phys. Soc. Japan*, **11**, 702–9.

Sato, H. 1959 *J. Phys. Soc. Japan*, **14**, 1797–1810.

Sato, H. 1960 *J. Fluid Mech.* **7**, 53–80.

Schade, H. & Michalke, A. 1962 *Z. Flugwiss.* **10**, 147–54 (also AFOSR Tech. Note no. 3191).

Schubauer, G. B. & Skramstad, H. K. 1947 *Nat. Bur. Stand. Res. Paper* RP-1772.

Tatsumi, T. & Kakutani, T. 1958 *J. Fluid Mech.* **4**, 261–75.

Watson, J. 1962 *J. Fluid Mech.* **14**, 211–21.

Wehrmann, O. 1960 *Deutsche Versuchsanstalt f. Luftfahrt, Porz-Wahn*, DVL-Rep. no. 131.

Wehrmann, O. & Wille, R. 1958 *Boundary Layer Research* (ed. H. Görtler), pp. 387–404. Berlin–Göttingen–Heidelberg: Springer-Verlag.

Wille, R. 1963 *Z. Flugwiss.* **11**, 222–33.